06

Effect of proton irradiation on the structure and properties of ZrO₂ powders and ceramics

© D.R. Belichko, G.K. Volkova, A.V. Maletckii, R.Sh. Isaev, M.N. Yakimenko, A.A. Zozulia

¹Galkin Donetsk Institute for Physics and Engineering,

283048, Donetsk, Russia

²International intergovernmental scientific research organization "Joint Institute for Nuclear Research",

141896 Dubna, Moscow Region, Russia

e-mail: danil.belichko@yandex.ru

Received March 28, 2025 Revised May 6, 2025 Accepted May 12, 2025

The results of a study of the effects of proton irradiation with an energy of $E_p = 2\,\text{MeV}$ and a dose of $D_p = 1 \cdot 10^{-17}\,\text{ion/cm}^2$ on oxide powders of the composition $\text{ZrO}_2 + n\,\%\,\text{Y}_2\text{O}_3$ (where $n = 2, 3, 4, 8\,\text{mol}\%$) are presented. X-ray phase analysis revealed radiation-induced monoclinic-tetragonal transformation in compacts containing partially stabilized zirconium dioxide after irradiation with a proton stream. X-ray diffraction analysis revealed a change in the half-width of diffraction reflections in the compact structure of all the phases studied, regardless of the type of their crystalline structure. grids. The Brunauer-Emmett-Teller method, scanning electron microscopy, and dilatometry revealed an increase in the size of ZrO_2 particles during proton flux irradiation. It has also been established that an increase and an increase in porosity in the material is observed during irradiation.

Keywords: zirconia, nanopowders, ceramics, proton flux, irradiation.

DOI: 10.61011/TP.2025.08.61738.52-25

Introduction

Today, search for radiation-resistant materials is an important task that determines the future of progress of reactor material science, power engineering and aerospace industry as well as approaches and principles of immobilization of nuclear fuel [1–3]. At the same time, it is important to take into account that materials involved in the above-said tasks shall have high tribological and mechanical properties and be resistant to high temperatures and pressures [1,4].

Ceramics based on stabilized zirconia (ZrO_2) has high strength and wear resistance [5]. Its key advantage is polymorphism that provides high fracture toughness: a tetragonal-monoclinic phase transition in a crack area decelerates its propagation due to a larger specific volume of the monoclinic phase, thereby making the tetragonal ZrO_2 a promising structural material [6].

Besides, high concentration of oxygen vacancies gives the material ion conductivity and low thermal conductivity [7], thereby extending its application as a functional material.

Additional doping and transition to a submicron grain size causes formation of new structure types in the material [8–11] and reduction of a sintering temperature [12]. In this regard, it is interesting to study radiation resistance of oxide ceramic materials based on nanodispersed ZrO_2 powders.

There are data that allow regarding zirconia as a radiation-resistant material. For example, it is indicated in the paper [13] that fully stabilized zirconia is radiation-resistance due to a large number of intrinsic oxygen vacancies, which

allow recombination of defects that are formed during irradiation and prevention of amorphization of the material when being irradiated by heavy ions. It is shown in the paper [14] when irradiating the nanocrystalline $\rm ZrO_2$ with heavy ions, there is agglomeration of cluster defects (vacancies and interstitial sites). Radiation resistance is also contributed by influence of zirconia grains and their size. Thus, the studies [15] provide data, according to which, when achieving the crystallite sizes of 100 nm ang higher there is observed parity of formed defects and defects recombined (annihilated) at the boundaries.

However, at the same time, there are not experimental data that are aimed at complex investigation of the effects of radiation on the structure of the nanodispersed zirconia-based media and its influence on consolidated media of these powders.

In view of the above said, the aim of the present study is to investigate the effects of proton irradiation with power of 2 MeV and a dose of $1 \cdot 10^{17} \text{ ion/cm}^2$ on the powder compacts of the $\text{ZrO}_2 + n \% \text{Y}_2 \text{O}_3$ composition (n = 2, 3, 4, 8 mol%) and the ceramics formed based thereon.

Materials and research methods

The nanopowders for investigations were produced by chemical deposition from solutions of salts of zirconium oxychloride (ZrOCl $_2$ x8H $_2$ O) and yttrium nitrate (Y(NO $_3$) $_3$) at the room temperature. The powders were crystallized in air at the temperature of 1000 °C for 2 h.

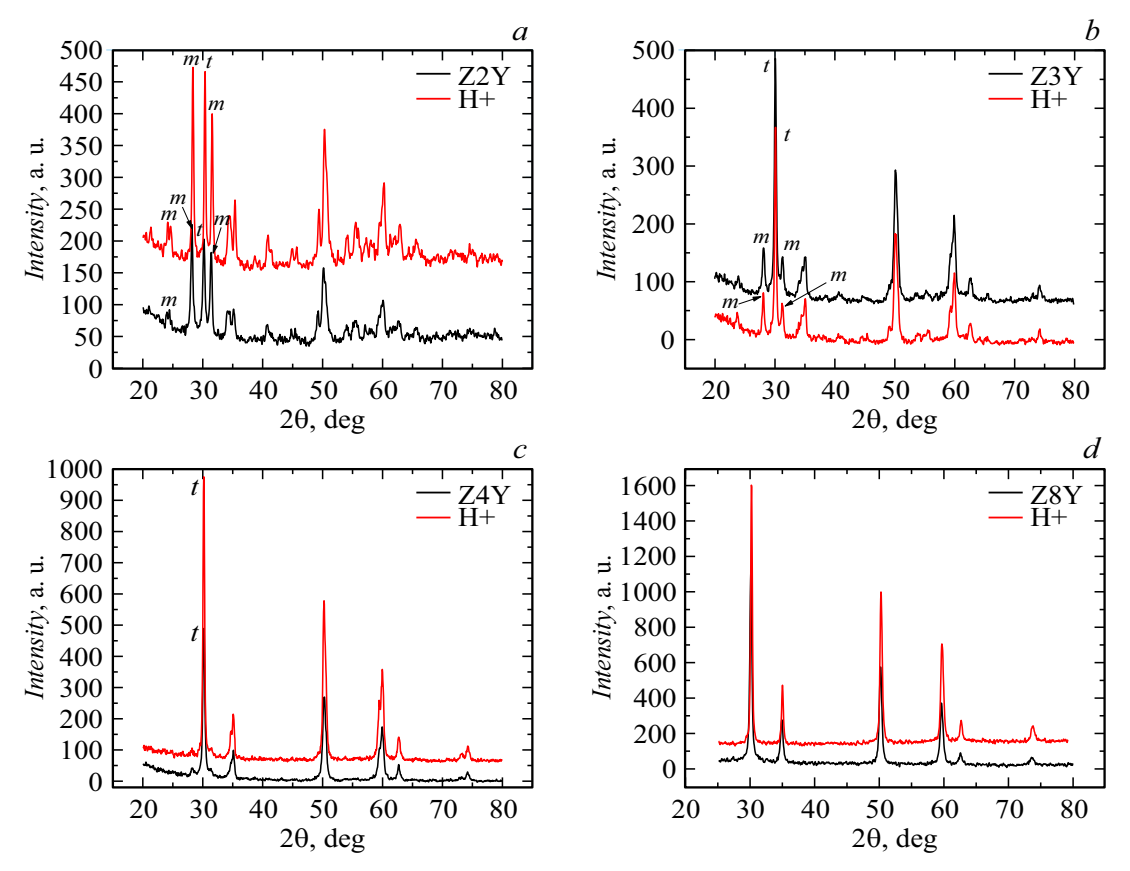


Figure 1. Diffraction patterns of the studied oxide systems before (black) and after (red) irradiation: a - Z2Y, b - Z3Y, c - Z4Y, d - Z8Y.

The CSR value of the powders was 32 nm. The powders were compacted by forming them in steel press forms under a load of 50 MPa with further processing by high hydrostatic pressure (HHP) of 400 MPa. The ceramics was synthesized by sintering the compacts at the temperature of 1500 °C with holding for 1 h in air. The concentration of the stabilizing impurity (Y₂O₃) was 2, 3, 4, 8 mol% (ZnY).

The produced powders were irradiated by means of the electrostatic accelerator EG-5. The dose power (D_p) was $1\cdot 10^{17}\,\mathrm{ion/cm^2}$ with the energy of 2 MeV.

X-ray diffraction analysis of the powders and the ceramics was carried out in the diffractometer DRON-3M in $\text{Cu}K_{\alpha}$ -radiation. A specific area of the powder surface was measured by the Brunauer-Emmett-Teller method (BET) in an instrument of the type "SORBI-4". A shrinkage degree of the sintered compacted pieces was measured by means of the dilatometer NETZSCH DIL 402 PC that was calibrated by the standard Al_2O_3 sample. The linear shrinkage of the pressed samples was measured by a constant heating rate methods within the range from the room temperature to 1500 °C at the heating rate of 5 °C/min. A sintering activation energy was calculated by a technique described in the paper [16,17].

The IR spectra of the nanopowders were recorded in the mid-IR range 400–4000 cm⁻¹ in the instrument Bruker Tensor 27. The powders were ground in a mortar together

with a spectroscopic-pure KBr powder. The concentration of the studied powders in mass was 0.5%.

The density (ρ) and the porosity (ε) of the synthesized ceramics were determined by a hydrostatic weighing method. The Vickers hardness (Hv) was determined in the hardness tester TP-7R-1 with a load of 30 kgf. The ceramics surface structure was studied in the scanning electron microscope (SEM) JEOL JSM 6510lv.

The measurement error was determined by a standard deviation method.

2. Research results

Fig. 1 shows X-ray diffraction patterns of the powder ZnY compacts before and after the effects of proton irradiation. The samples were synthesized by chemical deposition, annealed at the temperature of 1000 °C and compacted in the HHP conditions at 400 MPa.

It is clear from Fig. 1 that during irradiation there is an observed change of the phase composition of the initial dispersed materials — a monoclinic-tetragonal transformation. This effect is especially visual at the small concentrations of the stabilizing impurity (2 and 3 mol% of Y_2O_3), at which a difference of a mass content of the monoclinic modifications before and after irradiation is up to 10%. Table 1 shows dynamics of an amount of the monoclinic modification of

 Compacts
 Z2Y
 Z3Y
 Z4Y
 Z8Y

 Before irradiation
 75 %M+25 %T
 31 % M+69 %T
 9.5 % M+90.5 %T
 100 % C

 After irradiation
 65 % M+35 %T
 25.5 % C+74.5 %T
 5.5 % M+94.5 %T
 100 % C

Table 1. Phase composition of the ZnY compacts before and after irradiation by the proton flux

Note: M, T, C — monoclinic, tetragonal, cubic phases of ZrO₂, respectively, % are wt%.

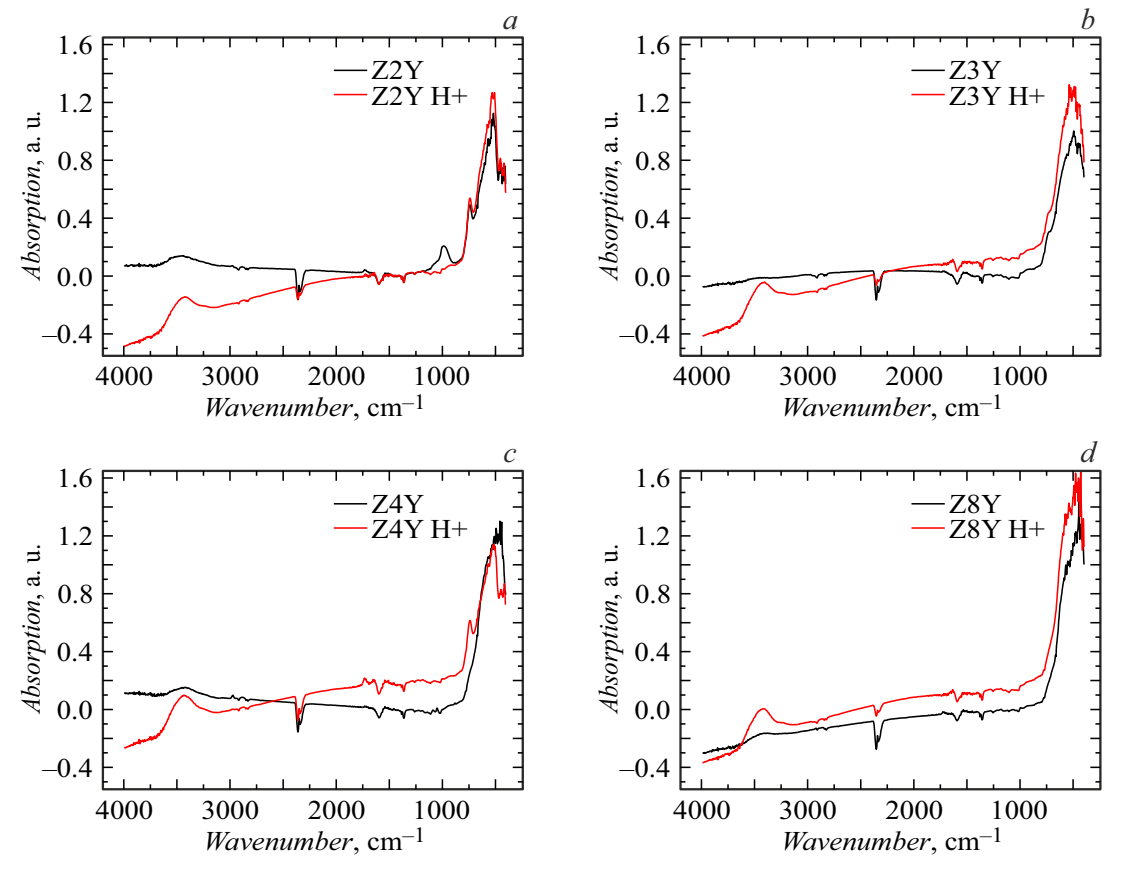


Figure 2. FIR spectra of the studied powder systems before (black) and after (red) irradiation: a - Z2Y, b - Z3Y, c - Z4Y, d - Z8Y.

	(hkl) of the phase peaks	Full width at half maximum, rad		
Sample		Before radiation	After radiation	
Z2Y	(11 1) M	0.006060	0.005232	
	(111) M	0.006452	0.005580	
	(101) T	0.005842	0.005232	
Z3Y	(101) T	0.006501	0.005336	
Z4Y	(101) T	0.005820	0.005188	
Z8Y	(111) C	0.006653	0.004687	

Table 2. Values of the components of physical broadening of β_{ε} of the studied ZrO₂ phases

Note. Error of determination of the full width at half maximum is $\pm 0.00002\,\text{rad}$

ZrO₂ depending on the concentration of a dopant under effects of ionizing irradiation.

Table 2 provides the values of the components of physical broadening of β_{ε} (that are responsible for lattice

Conditions	Z2Y	Z3Y	Z4Y	Z8Y
S _{bet} before irradiation, m ² /g	17.1 ± 0.2	15.9 ± 0.2	16.8 ± 0.2	17.8 ± 0.2
S_{bet} after irradiation, m^2/g	13.1 ± 0.2	15.5 ± 0.3	9.6 ± 0.1	12 ± 0.1

Table 3. Value of the specific surface area in the BET method for the nanopowders before and after proton irradiation

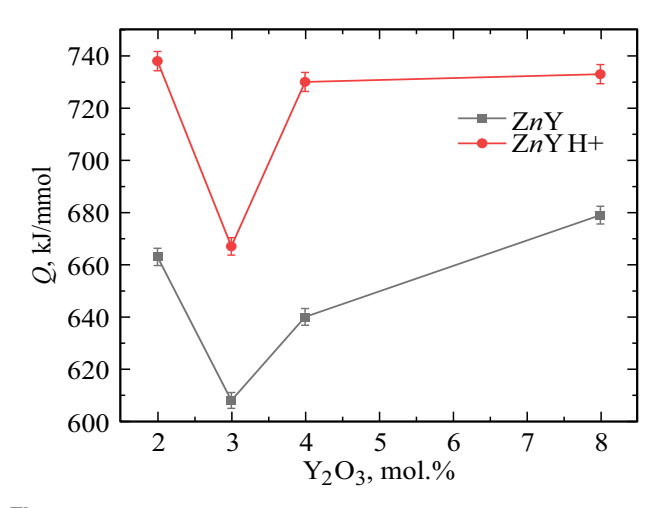


Figure 3. Sintering activation energy of the studied compacts before (black) and after proton irradiation (red).

microstrain) that are isolated from FWHM (Full Width at Half Maximum) of the studied ZrO₂ phases.

Fig. 2 shows the results of the IR Fourier spectroscopy of the powder systems of the ZnY composition before and after irradiation by protons with the energy of $E_p = 2 \text{ MeV}$ and the dose of $D_p = 1 \cdot 10^{17} \text{ ion/cm}^2$.

The powders of the ZnY composition after HHP of 400 MPa and proton irradiation were studied by a dilatometry method at the constant heating rate. Fig. 3 shows the values of the sintering activation energy of the compacts depending on the content of Y_2O_3 and proton irradiation.

It is clear from Fig. 3 that the irradiated compacts have the sintering activation energy that is higher by $8-10\,\%$ as compared to the initial materials.

Table 3 shows the values of the specific surface area of the studied dispersed materials before and after irradiation.

Fig. 4 shows a morphology of individual studied dispersed systems before and after proton irradiation.

It is clear from the microphotos of Fig. 4 that under effects of proton irradiation open porosity is formed in the compact structure and it increases.

Fig. 5 and Table 4 show the diffraction patterns of the phase composition of the ZnY ceramics produced by sintering of the initial and the proton-irradiated powders at $1500\,^{\circ}\text{C}$.

Fig. 6 shows values of density, porosity and hardness of the ceramics sintered at $1500\,^{\circ}$ C, depending on the content of Y_2O_3 and proton irradiation.

3. Discussion of the results

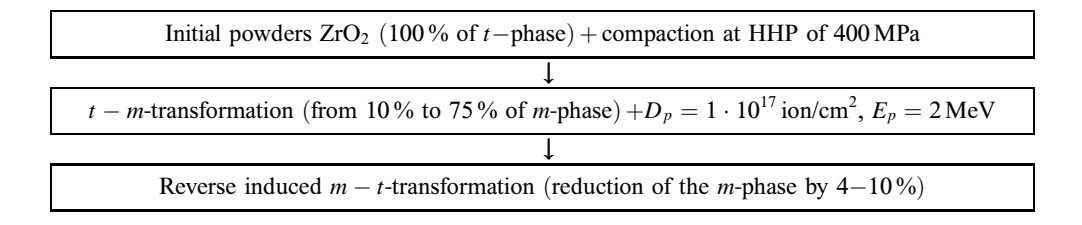
Two interrelated effects were found by the method of X-ray diffraction analysis (XDA) in the proton-irradiated compacts of the ZnY compositions (n = 2, 3, 4, 8 mol%): a radiation-induced monoclinic-tetragonal $(m \rightarrow t\text{-}ZrO_2)$ phase transformation and reduction of physical broadening of the diffraction peaks in all the ZrO₂ phases (Table 1). The difference in an amount of m-ZrO₂ is the higher, the less Y₂O₃ in the material, i.e. in a more metastable state the initial matrix is. The said $m \leftrightarrow t\text{-}ZrO_2$ transformation is of a shear type, i.e. diffusionless, while kinetics of the transformation is determined by stresses that originate in restructuring with a change of the sample volume: with the $m \rightarrow t$ transformation the structure is compressed by 3.42 %, while in the reverse, $t \rightarrow m$ transformation, it is expanded [18]. It is transformed by moving the boundary within the plane (100) and this transformation is accompanied by twinning. The monoclinic ZrO₂ (S.G. P2_{1/c}) has a structure that is similar to the fluorite one, but it fundamentally differs from it by a septenary cation coordination.

The compacts of the ZnY powders (n = 2, 3, 4, 8 mol%) (HHP of 400 MPa) consist a mixture of the t- and m-ZrO₂ phases (Fig. 1, Table 1), wherein it is necessary to note that both the phases are in a stress-strain state, especially m-ZrO₂, whose structures is characterized as a strain monoclinic martensite. The said compacts were irradiated by protons of $E_p = 2 \text{ MeV}$ with $D_p \ 10^{17} \text{ ion/cm}^2$.

Proton irradiation with the energy of 2 MeV induces formation of point defects — Frenkel pairs (an interstitial atom and a respective vacancy) in ZrO₂. Stability of these pairs depends on the imparted kinetic energy: with insufficient energy, recombination takes place, whereas stable pairs that occur as a result of elastic interaction form a new defect structure and affect its interaction with the structure that already exists in the initial matrix.

Effects of protons result in formation of heterogeneous defects, their mutual transformation and restructuring, which in some cases can cause phase transitions. The key effects of proton irradiation [19] include: decomposition of solid solutions with subsequent migration of components, formation of pores (including nanopores) as well as a directional flow of the point defects to drains (grain boundaries, pores, etc.), which results in origination of concentration gradients.

Taking into account all the processes in the material starting from the initial powder, an entire chain of the phase transformations can be schematically depicted:



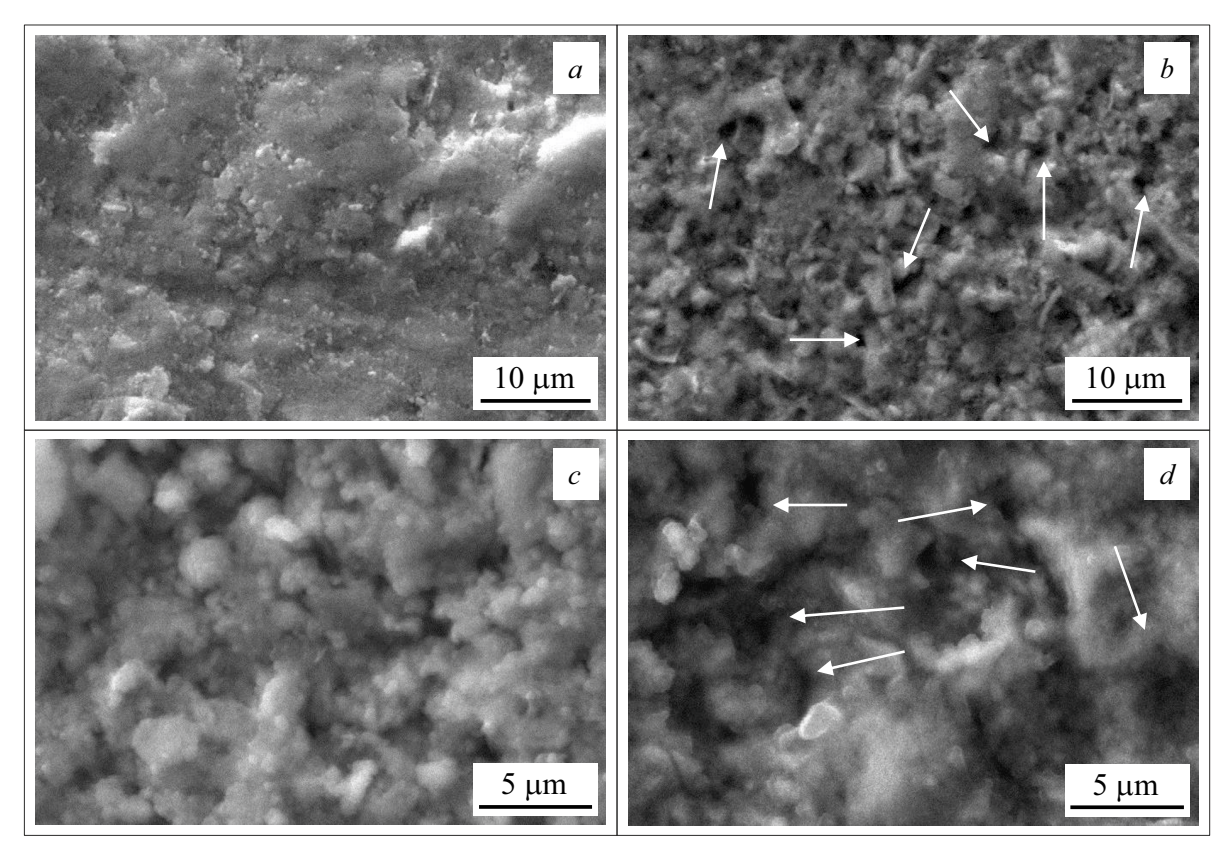


Figure 4. Morphology of the surface of the studied compacts before and after irradiation: a - Z2Y before irradiation, b - Z2Y after irradiation, c - Z4Y before irradiation, d - Z4Y after irradiation. The arrows mark pores that are formed during irradiation.

Table 4. Phase composition of the studied ceramics produced from the initial and the irradiated powders

Ceramics	Z2Y	Z3Y	Z4Y	Z8Y
From the initial powders	4.5 % M+95.5 % T	9.5 % C+90.5 % T	15 % C+85 % T	100 % C
From the irradiated powders	5.5 % M+94.5 % T	10 % C+90 % T	13 % C+87 % T	100 % C

Explanation of the found radiation-induced $m-t\text{-}ZrO_2$ transformation requires taking into account the entire set of processes and phenomena that occur in the matrix as a results of the effects of proton irradiation.

It is known that during irradiation there is acceleration of diffusion processes of two opposite flows of point defects — interstitial sites and vacancies, which move to drains at different speeds.

The diffusion speed of the interstitial sites is always higher than that of the vacancies, wherein it is inversely proportional to their atomic radius.

Proton irradiation can cause decomposition of the solid solution of yttrium in zirconia with further diffusion of yttrium to defect drains. In the solid solution of ZnY, yttrium is an over-dimensional element $(r(Y^{3+}) = 0.97 \text{ Å})$ for the coordinate number 6, as compared to $r(Zr^{4+}) = 0.82 \text{ Å})$ [20].

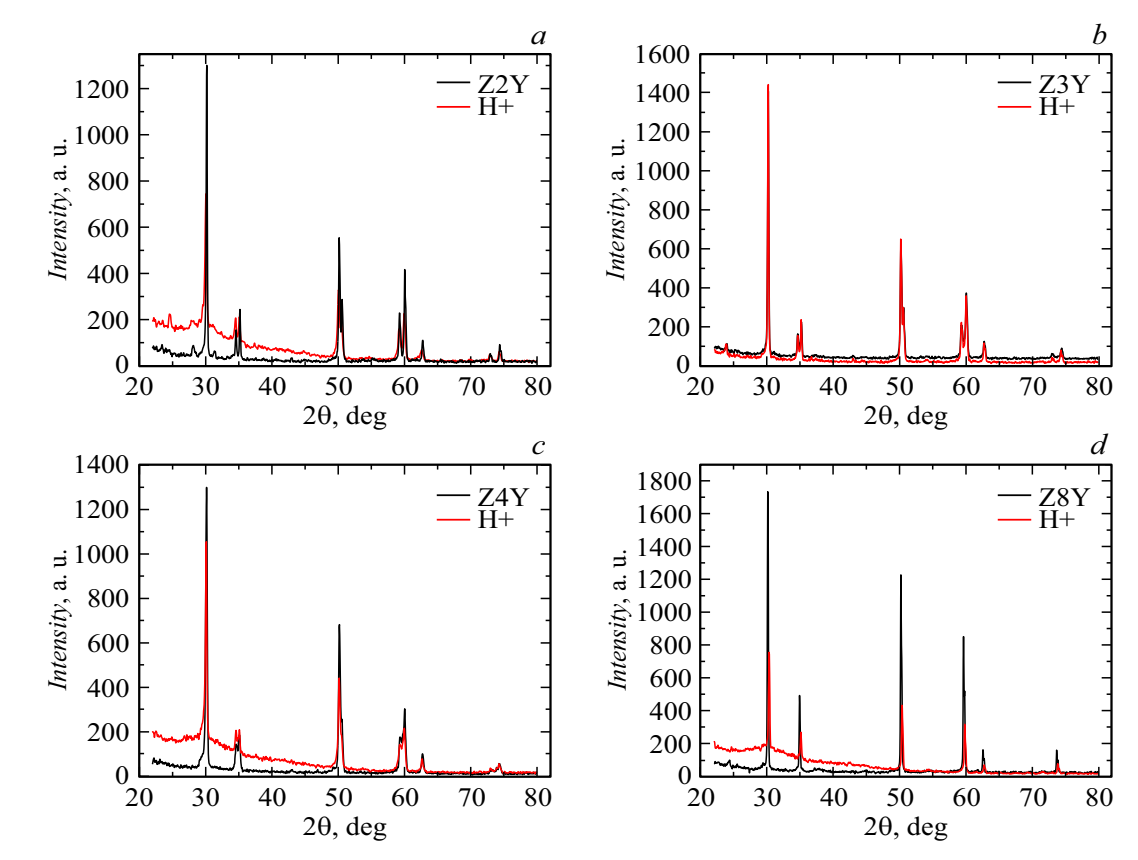


Figure 5. Diffraction patterns of the ceramic samples produced from the irradiated (red) and the initial (black) compacts: a - Z2Y, b - Z3Y, c - Z4Y, d - Z8Y.

And, therefore, drain boundaries will be yttrium-depleted. However, in the materials with an observed concentration gradient by any element, yttrium-enriched areas are close to the depleted areas and adjacent to them. The yttrium-enriched portions stabilize the *t*-phase, while, vice versa, the depleted portions destabilize it.

According to a diagram of states of $ZrO_2-Y_2O_3$ [21], at the concentration $Y_2O_3=8\,\mathrm{mol}\%$ there is complete stabilization of ZrO_2 to the cubic state (S.G. Fm3m) with the fluorite structure. Because of this, the cubic zirconia is phase-stable to all the external effects, including proton irradiation (Table 1). The minimum stability to proton radiation is recorded in the Z2Y system. The greatest stability was also demonstrated by the compact of the Z4Y composition, whereas the mean stability to the m-t-transition corresponded to the Z3Y composition.

It was shown by XDA of the ceramics $(1500 \,^{\circ}\text{C}, 1 \, \text{h})$ (Fig. 5) produced from the irradiated and the non-irradiated compacts that in both the cases the phase composition is identical within an error (Table 4).

The second key result of XDA of the influence of proton irradiation on a fine structure of the compacts of all the studied compositions is reduction of Full Width at Half Maximum (Table 2) (diffraction FWHM) of all the ZrO_2 phases in the irradiated samples as compared to the non-

irradiated samples [22]. This effect was previously observed in the irradiated ceramics [23].

The identified effect was analyzed to indicate interaction of the radiation-induced defects with the initial defects of the material. The existing defects create local stresses in the crystal lattice: the interstitial atoms cause distortions that propagate for at least 5 coordination spheres [19], wherein their influence substantially exceeds the effects induced by the vacancies.

Fields of the local stresses with opposite signs, which are created by the heterogeneous defects result in their recombination during interaction. Moreover, proton irradiation results in acceleration of diffusion mobility of the point defects and increase of their number as well as in increase of internal defect drains. Both the factors facilitate annihilation of the point defects and their complexes and result in reduction of a level of the local stresses (stresses of the 2nd kind), thereby inevitably resulting in significant reduction of diffraction FWHM in all the ZrO₂ phases irrespective of the type of the crystal lattice.

Another effect of proton irradiation on the structure of the powder compacts of the ceramics is a change of their physical properties: the change of the sintering activation energy (Fig. 3), reduction of the density (Fig. 6), reduction of the specific surface area (Table 3). All these effects are

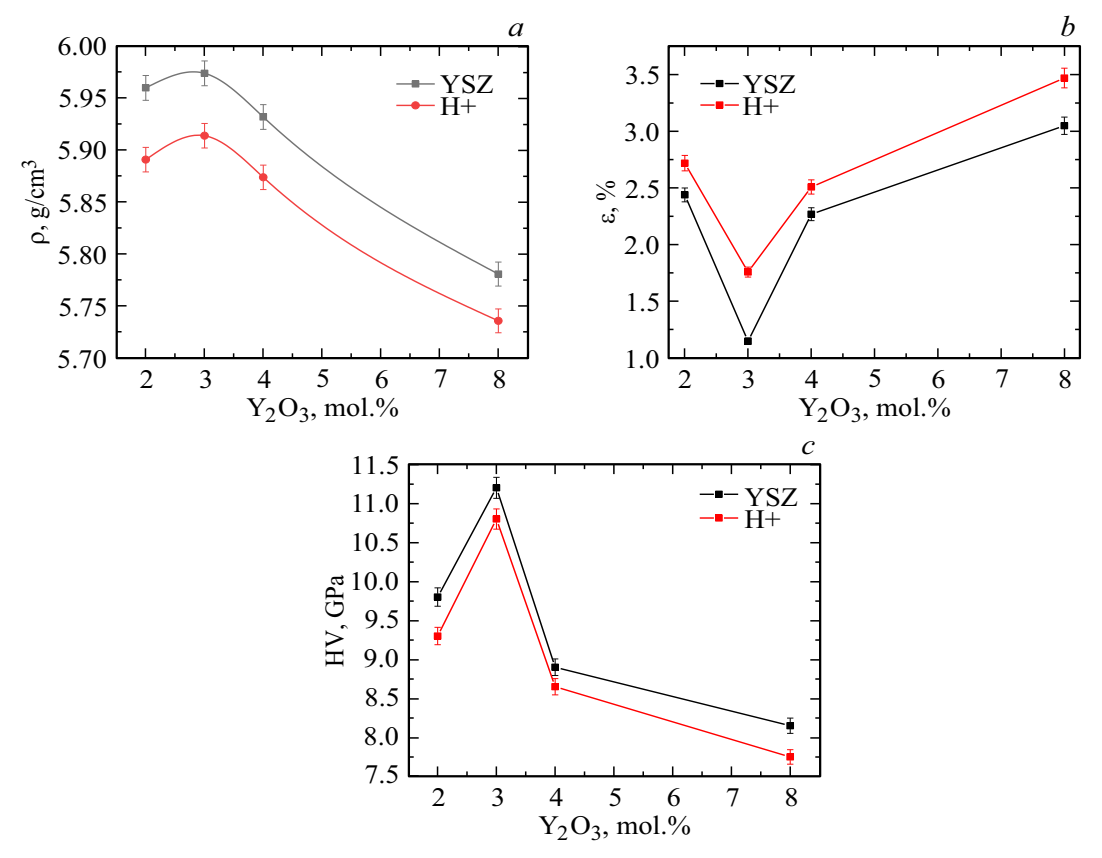


Figure 6. Values of the density (a), the porosity (b) and the hardness (c) of the studied ceramics produced from the initial compacts (black) and the proton-irradiated compacts (red).

directly related to a growth of porosity in the compacts and an increase of the sizes of the ZrO_2 particles.

The results of IR Fourier spectroscopy (Fig. 2) confirm adsorption of water and CO_2 on the irradiated compacts. The bands $3400\,\mathrm{cm}^{-1}$ (OH-groups) and $1600\,\mathrm{cm}^{-1}$ (H₂O) are more intense for the irradiated samples, thereby indicating accelerated adsorption. The carbonate peaks $(1361-1386\,\mathrm{cm}^{-1})$ and occluded CO_2 (2355 cm⁻¹) are also observed and they are more pronounced for the non-irradiated samples. The weak peaks $(2830-2900\,\mathrm{cm}^{-1})$ correspond to the C-H-oscillations. These effects are related to the growth of open porosity (Fig. 4, Fig. 6, *b*), which also explains reduction of ceramics hardness (Fig. 6, *c*).

The increase of the values of the sintering activation energy and reductions of the specific surface area in the BET method are due to the change of the particle sizes (increase of them). The specific surface area of the dispersed materials is inversely proportional to the particle sizes. The change of the sintering activation energy is related to the change of a predominant sintering mechanism (volume diffusion and grain-boundary diffusion). According to the papers [23,24], the sintering mechanism and the energy of its activation is caused by a ratio of the particle surface to its volume — with reduction of the particle sizes the mechanism of volume diffusion is predominant. The increase of the sintering activation energy directly indicates

a change of the ratio of the particle surface to the volume, which correlates with reduction of the specific surface area of the compacts.

It should be also noted that a change of the -OH absorption band and the sintering activation energy may be caused by radiation-induced processes in the material — radiolysis of water. If the material contains traces of water (adsorbed on the surface or in the pores), proton irradiation causes its decomposition: the proton energy "breaks" the H_2O molecules into reactive radicals (H_1 , OH_2). Hydroxyl radicals can join the material surface by forming the OH-groups. With these groups on the surface of the particles, it results in reduction of the surface energy, which is a driving force of sintering.

Thus, the influence of proton irradiation on the ZnY compacts (n=2, 3, 4, 8 mol%) (HHP of 400 MPa) has been studied to identify a set of radiation effects: the radiation-induced phase transition due to decomposition of the Zr-Y solid solution with subsequent diffusion of ions, reduction of total defectiveness of the material, formation of open porosity, which result in adsorption of water and reduction of the density and the hardness of the sintered ceramics, as well as the crystallite growth causing reduction of the specific surface in the BET method and the increase of the sintering activation energy.

Conclusions

- 1. The XFA method has detected the radiation-induced monoclinic-tetragonal transformation in the powder compacts of the ZrO₂ + n% Y₂O₃ composition (n=2, 3, 4 mol%) after proton irradiation ($E_p=2$ MeV, $D_p=1\cdot 10^{17}$ ion/cm²), which is manifested in reduction of the content of m-ZrO₂ by 4–10 wt.% depending on the concentration of Y₂O₃.
- 2. It is demonstrated by the X-ray studies that the structure-sensitive characteristic of the rated diffraction reflections the physical width (β) in the tetragonal, monoclinic and cubic ZrO_2 phases in the irradiated compacted pieces at all the concentrations of Y_2O_3 is always less than in the initial ones.
- 3. The phase composition in the ceramics of the irradiated and the non-irradiated compacts is almost identical, but the structure in the irradiated ZrO_2 is more porous.
- 4. The methods of BET, XDA, SEM and dilatometry have shown that after proton irradiation the powder compacted pieces exhibited the increase of the powder particle sizes.
- 5. It is found that the most typical effects of proton irradiation are formation of pores in the irradiated material.
- 6. The Z3Y ceramics has demonstrated the best physical-mechanical characteristics: the samples made of the initial powder had $\rho = 5.97\,\mathrm{g/cm^3}$, $\varepsilon = 1.15\,\%$, HV = 11.2 GPa; while the samples of the irradiated powder had $\rho = 5.91\,\mathrm{g/cm^3}$, $\varepsilon = 1.7\,\%$, HV = 10.8 GPa.

Funding

The studies were supported by RSF, grant № 24-72-10072, https://rscf.ru/project/24-72-10072/

Conflict of interest

The authors declare that they have no conflict of interest.

References

- [1] A.M. Abd El-Hameed. NRIAG J. Astronomy Geophys., **11** (1), 313 (2022). DOI: 10.1080/20909977.2022.2079902
- [2] F. García Ferr'e, A. Mairov, L. Ceseracciu, Y. Serruys, P. Trocellier, C. Baumier, O. Kaïtasov, R. Brescia, D. Gastaldi, P. Vena, M.G. Beghi, L. Beck, K. Sridharan, F. Di Fonzo. Sci. Rep., 6, 33478 (2016). https://doi.org/10.1038/srep33478
- [3] R. Devanathan, K.E. Sickafus, W.J. Weber, M. Nastasi. J. Nucl. Mater., 253 (1-3), 113 (1998). https://doi.org/10.1016/S0022-3115(97)00307-3
- [4] J. Chai, Y. Zhu, L. Niu, T. Shen, M. Cui, Z. Wang. Ceram. Int., 49 (20), 32799 (2023). https://doi.org/10.1016/j.ceramint.2023.07.249
- [5] A.A. Dmitrievsky, D.G. Zhigacheva, N.Y. Yefremov, P.N. Ovchinnikov, V.M. Vasyukov. Solid State Physics, 64 (8), 1018 (2022). DOI: 0.21883/FTT.2022.08.52700.355
- [6] A.A. Leonov, E.V. Abdulmenova, M.P. Kalashnikov, Li Jing. Mater. Sci. Issues, 4 (104), 132 (2020).
 DOI: 10.22349/1994-6716-2020-104-4-132-143

- J. Chevalier, L. Gremillard, A.V. Virkar, D.R. Clarke. J. American Ceramic Society, 92 (9), 1901 (2009).
 DOI: 10.1111/j.1551-2916.2009.03278.x
- [8] D.R. Belichko, T.E. Konstantinova, G.K. Volkova, M.N. Mirzayev, A.V. Maletsky, V.V. Burkhovetskiy, A.S. Doroshkevych, C. Mita, D.M. Mardare, B. Janiska, Asif Nabiyev, A.I. Lyubchyk, A.A. Tatarinova, E. Popov. Mater. Chem. Phys., 287 (1), 126237 (2022).
 DOI: 10.1016/j.matchemphys.2022.126237
- [9] D.R. Belichko, T.E. Konstantinova, A.V. Maletsky, G.K. Volkova, A.S. Doroshkevych, M.V. Lacusta, M. Kulik, A.A. Tatarinova, D. Mardare, C. Mita, N. Cornei. Ceram. Intern., 47 (3), 3142 (2021). DOI: 10.1016/j.ceramint.2020.09.151
- [10] V. Ivanov, S. Shkerin, A. Rempel, V. Khrustov, A. Lipilin, A. Nikonov. J. Nanosci. Nanotechnol., 10 (11), 7411-5 (2010). DOI: 10.1166/jnn.2010.2836. PMID: 21137947
- [11] D.R. Belichko, G.K. Volkova, T.E. Konstantinova, A.V. Maletsky. FTVD, 33 (2), 1 (2023).
- [12] N. Takahashi, A. Suda, I. Hachisuka, M. Sugiura,
 H. Sobukawa, H. Shinjoh. Appl. Catalysis B: Environmental,
 72 (1-2), 187 (2007). DOI: 10.1016/j.apcatb.2006.10.014
- [13] G. Pu, J. Zou, L. Lin, K. Zhang, B. Liu, F. Ma, Q. Wang,
 Q. Li. J. Alloys Compounds, 18 (771), 13150 (2018).
 DOI: 10.1016/j.jallcom.2018.08.259
- [14] J. Liua, A.H. Mir, G. He, M. Danaie, J. Hinks, S. Donnelly, H. Nordin, S. Lozano-Perez, C.R.M. Grovenor. Acta Mater., 199, 429, (2020). https://doi.org/10.1016/j.actamat.2020.08.064
- [15] F. Lu, J. Zhang, A. Navrotsky, R.C. Ewing, J. Lian. Microscopy Society of America, 16 (2), 1624 (2010). DOI: 10.1017/S1431927610062069.
- [16] A.V. Maletskyi, G.K. Volkova, D.R. Belichko, V.A. Glazunova, A.S. Doroshkevych, A.A. Tatarinova, S.I. Lyubchyk. Ceram. Intern., 50 (22), 46506 (2024). DOI: 10.1016/j.ceramint.2024.09.002
- [17] M. Lakusta, I. Danilenko, T. Konstantinova, G.Volkova. Nanoscale Res. Lett., 11 (1), 11671 (2016). DOI: 10.1186/s11671-016-1452-3
- [18] V.N. Strekalovskii. Oksidy s primesnoi razuporyadochennost'yu. Sostav, struktura, phasovye prevrashcheniya (Nauka, M., 1987), s. 158 (in Russian).
- [19] V.V. Uglov. *Radiatsionnye protsessy i yavleniya v tverdykh telakh* (Vysheishaya shkola, Minsk, 2016), s. 188 (in Russian).
- [20] B.K. Vainshtein. Sovremennaya kristallografiya (Nauka, M., 1979), t. 2, s. 384 (in Russian).
- [21] D.O. Julián, L. Adrián, T. Alejandro, P.H. Juan. Dyna, 81 (185), 13 (2014). https://www.redalyc.org/articulo.oa?id=49631031002
- [22] A.I.Gusev. Nanomaterialy, nanostruktury, nanotekhnologii (Fizmatlit, M., 2005), s. 416 (in Russian).
- [23] D.R. Belichko, G.K. Volkova, A.V. Maletsky, I.Sh. Isaev, Mater. Sci. Issues, 3 (119), 46 (2024). https://doi.org/10.22349/1994-6716-2024-119-3-46-56
- [24] I. Danilenko, M. Lakusta, L. Loladze, G. Volkova, I. Popov, V. Glazunova, T. Konstantinova. Results in Physics, 19, 103495 (2020). https://doi.org/10.1016/j.rinp.2020.103495

Translated by M.Shevelev